AIChE

Frequency Response Analysis of Slot Coating

Takeaki Tsuda
Dai Nippon Printing Co., Ltd., Technology Development Center, Tsukuba Ibaraki 300-2646 Japan

Juan M. de Santos
Avery Dennison Corp., Avery Research Center, 2900 Bradley St., Pasadena, CA 91107

L. E. Scriven
Dept. of Chemical Engineering and Material Science, University of Minnesota, Minneapolis, MN 55455

DOI 10.1002/aic.12150
Published online February 9, 2010 in Wiley Online Library (wileyonlinelibrary.com).

Frequency responses to the slot die coating process is analyzed using empirical modal analysis to predict the effects of periodic process disturbances such as gap oscillation and variations in vacuum *pressure, web velocity, and flow rate. A type of empirical modal analysis known as an experimental modal approach was used, and an oscillator basis model was assumed by using a linearized governing equation, and the coefficient of the basis model was determined by curve-fitting. By completing the process, we were able to decompose each mode, during which process it was found that the modes are of two types: a squeeze mode related to viscous characteristics and sinuous modes that are identical to capillary waves. Observation of the meniscus shapes of each mode revealed, in the third mode near the lip edge, significant fluctuations that can induce other coating defects.* © 2010 American Institute of Chemical Engineers
AIChE J, 56: 2268–2279, 2010
Keywords: coating flows, fluid mechanics, numerical solutions

Introduction

Slot die coating is often used to produce coatings of highly accurate and uniform thickness, such as photographic films, magnetic tapes, and optical filter sheets.[1] When producing coatings with tight specifications, slight dynamic mechanical disturbances such as gap oscillations and variations *in vacuum* pressure, web velocity, and flow rate of the coating liquid have deleterious effects on the coating bead and meniscus, resulting in coating defects such as barring, streaks, swelling, and air entrainment as shown in Figure 1.[1]

Two approaches exist for avoiding these coating defects. One is to thoroughly review the integrity of the process, such as the die geometry and the characteristics of the coating liquid. The other is to optimize operational parameter settings such as coating gap, vacuum pressure, web velocity, and flow rate of the coating liquid. Since the magnitude of the coating defects due to periodic disturbances depends on frequency of those disturbances, one must examine innumerable combinations of settings to determine what combination most effectively decreases the sensitivity of the process to disturbances.[2]

To evaluate process sensitivity to disturbances, an experimental approach is often used.[3] However, as previously suggested, such an approach is generally expensive. In contrast, with a reliable theoretical model, many aspects of coating quality can be computed over large ranges of frequencies at relatively low cost. Theoretical models are rarely complete, but can be validated by comparing their calculated predictions with experimental results.

Generally, the response of a flow to external disturbances is predicted by computing an equation system linearized around a steady-state value; in modern control theory, this approach is called the state-space formalism.[4] Van

Correspondence concerning this article should be addressed to T. Tsuda at Tsuda-T2@mail.dnp.co.jp.

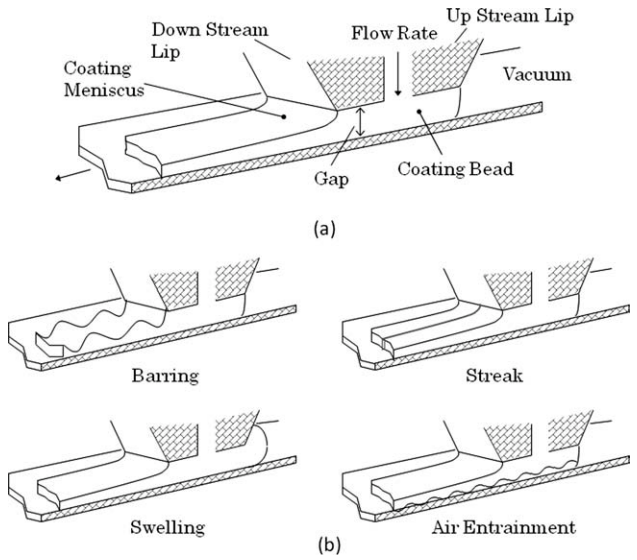

Figure 1. Typical slot coating configuration: (a) Operational parameters, and (b) Coating defects.

Abbenyen[5] and Christodoulou[6] introduced this approach to predict the frequency response of slide coating using the Galerkin finite element method for a two-dimensional (2-D) Navier-Stokes system. Later, Cai[7] and Gates[8] applied the approach to slot coating and Musson[9] further applied it to two-layer slot coating.

An alternative way to predict the response of a flow to external disturbances is to solve the transient Navier-Stokes equation. Katagiri and Scriven[10] used this approach to analyze the frequency response of slide coating to oscillations in flow rate and showed that theoretical-frequency-response analysis is an effective way to model coating flow problems. However, to compute the equation system requires that a large matrix system be solved at each disturbance frequency. Therefore, in terms of time cost, this approach is not particularly efficient for handling every coating flow problem. Furthermore, these studies are limited in two ways. First, system response to disturbances was evaluated solely in terms of final thickness. Second, a single peak in the frequency domain was regarded as representing one physical mode without allowing for any decomposition of modes.

To predict coating flow more efficiently, Landau and Levich[11] derived a classical film profile equation for the rising film in order to obtain the final thickness of the coated film on the moving wall. Gardner and Adebiyi[12] and Higgins[13] developed a 1-D theoretical visco-capillary model in which viscous and capillary forces are balanced over a 2-D cross section of the coating bead of the slot coating at steady state. Kheshgi[14] used this approach to develop a film profile equation that uses a 1-D momentum steady-state Navier-Stokes equation integrated in the depth direction to average each momentum term, similar to the approach of von Karman's integral momentum equation.[15] This approach agrees well with experimental values.[16] Kapitza[17] and Shkadov[18] used the boundary-layer approach, and Shkadov developed a two-field model involving film thickness and local flow rate, for which the velocity field is not supposed to be entirely slaved to the film thickness evolution. Other researchers, e.g.,[19] followed and continued to develop this approach. However, there are few reported cases of unsteady equation systems for frequency response analysis of slot coating.

In this article, we examine the frequency-response characteristics of slot coating using an empirical modal analysis known as the experimental modal approach, and devise an unsteady visco-capillary equation system.

One-dimensional unsteady equation

The Navier-Stokes system of conservation for unsteady flow, viewed in 2-D, is approximated by neglecting certain viscous stress terms that have little effect on nearly rectilinear flow[15] such as coating bead and meniscus, as

$$\rho\left(\frac{\partial u}{\partial t}+\frac{\partial u^2}{\partial x}+\frac{\partial uv}{\partial y}\right)=-\frac{\partial p}{\partial x}+\mu\frac{\partial^2 u}{\partial y^2} \tag{1}$$

where u,v are the components of velocity in the x,y directions, p is the static pressure, μ is the viscosity of the coating liquid, and ρ is the density of the liquid. To obtain a simplified 1-D equation, we average the momentum over the depth $h(x,t)$ of the liquid by integrating the equation as described by Higgins[13] and Kheshgi.[14] Integrating the y-component of the momentum equation yields

$$\int_0^h \rho\left(\frac{\partial u}{\partial t}+\frac{\partial u^2}{\partial x}+\frac{\partial uv}{\partial y}\right)dy=\int_0^h\left(-\frac{\partial p}{\partial x}+\mu\frac{\partial^2 u}{\partial y^2}\right)dy \tag{2}$$

We then integrate Eq. 2 by applying the Leibniz Integral rule to acceleration and inertial terms to obtain

$$\rho\left[\frac{\partial Q}{\partial t}-u(h)\frac{\partial h}{\partial t}+\frac{\partial}{\partial x}\int_0^h u^2dy-u^2(h)\frac{\partial h}{\partial x}+(uv_{y=h}-uv_{y=0})\right]=-h\frac{dp}{dx}+\left(\mu\frac{\partial u}{\partial y_{y=h}}-\mu\frac{\partial u}{\partial y_{y=0}}\right) \tag{3}$$

where Q is the volumetric flow rate. To solve this equation, we derive the lubrication-type velocity at unsteady state.

Generally, unsteady flow in the coating bead and meniscus can be divided into four types.[20] Figure 2 shows that each type of oscillation disturbance that induces coating defects creates an unsteady flow component, categorized as either Couette or Poiseuille flow. If we assume that each velocity is fully developed, the superposition principle becomes available to the velocity components as a quasi-steady model, and we obtain the velocity profile for the coating bead and meniscus as

$$u=\chi(x,y,t)+\xi(x,t)\psi(x,y,t) \tag{4}$$

where χ is the Couette component and ψ is the Poiseuille component, defined, respectively as

$$\chi=U(t)(1-y/h(x,t)) \tag{5}$$

$$\psi=y^2/2-h(x,t)y/2 \tag{6}$$

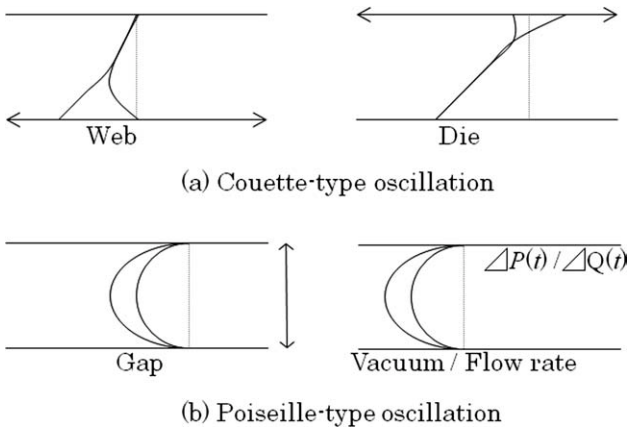

Figure 2. Typical flow types induced by oscillation disturbances.

Integrating Eq. 4 over the depth of the liquid gives the local flow rate Q and the time-dependent function ξ, defined as

$$\xi = \frac{12}{h(x,t)^3}\left(\frac{U(t)h(x,t)}{2} - Q(x,t)\right) \tag{7}$$

The local flow rates Q in each region except the slot region are defined by the flow rate at certain points and location parameters shown in Figure 3

$$Q_0(x,t) = F_0(t) - \frac{\partial}{\partial t}\int_{x_1}^{x} h dx \tag{8}$$

$$\begin{aligned} Q_1(x,t) &= F_1(t) + \frac{F_0(t) - F_1(t)}{L_1}(x - x_1 + L_1) \\ &= Q_i - \frac{dA_2}{dt} - \frac{1}{L_1}\frac{dA_1}{dt}(x - x_1 + L_1) \end{aligned} \tag{9}$$

$$\begin{aligned} Q_2(x,t) &= F_3(t) + \frac{F_2(t) - F_3(t)}{L_2 - x_4}(x - x_4) \\ &= -\frac{1}{L_2 - x_4}\frac{dA_2}{dt}(x - x_4) \end{aligned} \tag{10}$$

Where

$$\frac{dA_1}{dt} = F_1(t) - F_0(t), \quad \frac{dA_2}{dt} = F_3(t) - F_2(t)$$
$$F_1(t) = Q_i(t) + F_2(t) = Q_i(t) - \frac{dA_2}{dt}, \quad F_3(t) = 0$$

where A is the cross-sectional area of coating bead in each region, F is the local flow rate at a certain fixed point, and Q_i is the flow rate from the slot. In the slot region ($x_3 < x < x_2$), it is difficult to evaluate the velocity profile since the vertical velocity component must be taken into account. Instead, we assume a control volume not previously considered, so the conservation-of-momentum condition becomes

$$-\int_s \rho VV \bullet nds + \int_s n \bullet Tds = 0 \tag{11}$$

where V is the velocity vector, n is a normal vector, and T is the stress tensor. The inertial and viscous terms then become approximately

$$-\int_s \rho VV \bullet nds \cong \int_0^{h_u} \rho u(x_3)^2 dy - \int_0^{h_d} \rho u(x_2)^2 dy \tag{12}$$

$$\int_s n \bullet Tds \cong h_u p(x_3) - h_d p(x_2) - \int_{x_3}^{x_2} \tau_{yx} dx_{y=0} \tag{13}$$

By incorporating Eqs. 12 and 13, Eq. 11 becomes

$$\int_0^{h_u} \rho u(x_3)^2 dy - \int_0^{h_d} \rho u(x_2)^2 dy + h_u p(x_3) - h_d p(x_2) - \int_{x_3}^{x_2} \tau_{yx} dx_{y=0} = 0 \tag{14}$$

In the meniscus region, instead of using pressure drop dp/dx, we use the Young and Laplace equation, which defines the relationship between the mean radius of curvature of an interface and the pressure difference across an interface, since the pressure jump across a curved interface is equivalent to the meniscus pressure.[13] This gives

$$-\frac{dp}{dx} = \sigma\frac{d}{dx}\frac{1}{\kappa} = \sigma\frac{dH}{dx} = \sigma\frac{d}{dx}\left[\frac{h_{xx}}{(1 + h_x^2)^{3/2}}\right] \tag{15}$$

where κ is the radius of curvature of the meniscus, σ is the surface tension, and H is the curvature of meniscus. Using these equations and the kinematic condition (Eq. 16), we linearize Eq. 3 with respect to time derivatives to obtain

$$v = \frac{\partial h}{\partial t} + u\frac{\partial h}{\partial x} = h_t + uh_x \tag{16}$$

$$\sigma\frac{d}{dx}\left[\frac{h_{xx}}{(1 + h_x^2)^{3/2}}\right] = f_{\text{steady}}(x) + f_{\text{unsteady}}(x,t) \tag{17}$$

where

$$f_{\text{steady}} = \rho h_x\left(\frac{1}{5}\frac{U^2}{h} - \frac{6}{5}\frac{F_0^2}{h^3}\right) - 3\mu\left(\frac{U}{h^2} - \frac{F_0}{h^3}\right) \tag{18}$$

$$f_{\text{unsteady}} = \frac{\rho}{h}\left(F_{0t} - \frac{\partial^2}{\partial t^2}\int_{x_1}^{x} h dx\right) + \rho\left[h_{ta}\left(\frac{2}{5}\frac{U}{h} - \frac{12}{5}\frac{F_0}{h^2}\right) + \frac{\partial}{\partial t}\int_{x_1}^{x} h dx h_x \frac{12}{5}\frac{F_0}{h^3}\right] - \mu\frac{3}{h^3}\frac{\partial}{\partial t}\int_{x_1}^{x} h dx \tag{19}$$

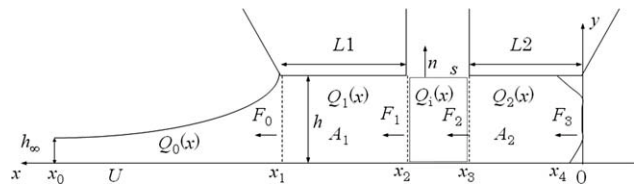

Figure 3. Configuration of local flow rate and parameters in the coating bead and meniscus.

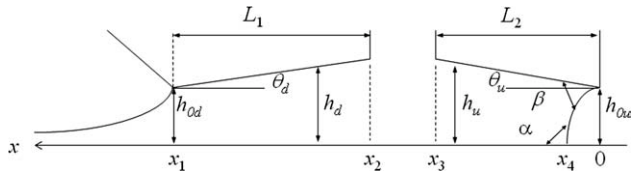

Figure 4. Configuration of upstream and downstream lips in coating bead region.

$$h_{ta} = h_t - h_t(x_1) \tag{20}$$

In the coating bead region, we consider inclined upstream and downstream lips, which are typical techniques used to improve coating quality (Figure 4).

The equation for the upstream region ($x_4 < x < x_3$), derived by substituting in Eq. 3, is

$$-\frac{\partial p}{\partial x} = f_{\text{steady}}(x) + f_{\text{unsteady}}(x,t) \tag{21}$$

where

$$f_{\text{steady}} = \frac{\rho}{h_u}\frac{2}{15}U^2\tan\theta_u - \mu\frac{6}{h_u^2}U \tag{22}$$

$$\begin{aligned} f_{\text{unsteady}} &= \rho\frac{x-x_4}{h_u}\left(x_{4tt}\frac{h_{0u}+x_4\tan\theta_u}{L_2-x_4} - h_{0utt}\right) \\ &+ \frac{\rho}{h_u}\frac{1}{5}U\left(h_{0ut} - x_{4t}\frac{h_{0u}+x_4\tan\theta_u}{L_2-x_4}\right) \\ &- \mu\frac{12(x-x_4)}{h_u^3}\left(h_{0ut} - x_{4t}\frac{h_{0u}+x_4\tan\theta_u}{L_2-x_4}\right) \end{aligned} \tag{23}$$

$$h_u = h_{0u} + x\ \tan\ \theta_u \tag{24}$$

where the t and x subscripts indicate derivatives with respect to time and the x coordinate, respectively. The equation for the slot region ($x_3 < x < x_2$) is

$$h_d(x_2)p(x_2) - h_u(x_3)p(x_3) = f(x)_{\text{steady}} + f(x,t)_{\text{unsteady}} \tag{25}$$

where

$$\begin{aligned} f_{\text{steady}} &= \rho\left(\frac{2}{15}U^2(h_u(x_3)-h_d(x_2)) + \frac{1}{5}UQ_i - \frac{6}{5}\frac{Q_i^2}{h_d(x_2)}\right) \\ &+ \mu(x_2-x_3)\left[2U\left(\frac{1}{h_d(x_2)}+\frac{1}{h_u(x_3)}\right) - \frac{3}{h_d(x_2)^2}Q_i\right] \end{aligned} \tag{26}$$

$$\begin{aligned} f_{\text{unsteady}} &= \rho\frac{12}{5}\frac{Q_i}{h_d(x_2)}[h_{0ut}(L_2-x_4) - x_{4t}(h_{0u}+x_4\tan\theta_u)] \\ &+ 3\mu(x_2-x_3)\left(\frac{1}{h_d(x_2)^2}+\frac{1}{h_u(x_3)^2}\right) \\ &\times [h_{0ut}(L_2-x_4) - x_{4t}(h_{0u}+x_4\tan\theta_u)] \end{aligned} \tag{27}$$

$$h_d = h_{0d} - (x-x_1)\tan\theta_d \tag{28}$$

The equation for the downstream region ($x_2 < x < x_1$) is

$$-\frac{dp}{dx} = f(x)_{\text{steady}} + f(x,t)_{\text{unsteady}} \tag{29}$$

where

$$\begin{aligned} f_{\text{steady}} &= \rho\left(-\frac{2}{15}\tan\theta_d U^2\frac{1}{h_d} + \frac{6}{5}Q_i^2\tan\theta_d\frac{1}{h_d^3}\right) \\ &- \mu\left(\frac{6}{h_d^2}U - \frac{12}{h_d^3}Q_i\right) \end{aligned} \tag{30}$$

$$\begin{aligned} f_{\text{unsteady}} &= \rho\left\{\frac{1}{h_d}\frac{\partial Q_i}{\partial t} - \frac{1}{h_d}\left[h_{0utt}(L_2-x_4)\right.\right. \\ &\left.\left. - x_{4tt}(h_{0u}+x_4\tan\theta_u)\right] - h_{0dtt}\left[\frac{x-x_1+L_1}{h_d}\right]\right\} \\ &+ \rho\left\{-\frac{12}{5}Q_i\tan\theta_d\left[\frac{1}{h_d^3}(h_{0ut}(L_2-x_4) - x_{4t}(h_{0u}+x_4\tan\theta_u))\right.\right. \\ &\left.\left. + \frac{h_{0dt}}{h_d^3}(x-x_1+L_1)\right] + \left(\frac{1}{5}U - \frac{12}{5}\frac{Q_i}{h_d}\right)\frac{h_{0dt}}{h_d}\right\} \\ &- \mu\left\{\frac{12}{h_d^3}[h_{0ut}(L_2-x_4) - x_{4t}(h_{0u}+x_4\tan\theta_u)]\right. \\ &\left. + 12h_{0dt}\frac{(x-x_1+L_1)}{h_d^3}\right\} \end{aligned} \tag{31}$$

Using the parameter configuration in Figure 4, for F_0 in Eqs. 19, 20 we obtain

$$\begin{aligned} F_0 &= Q_i - A_{1t} - A_{2t} \\ &= Q_i - L_1h_{0dt} - h_{0ut}(L_2-x_4) + x_{4t}(h_{0u}+x_4\tan\theta_u) \end{aligned} \tag{32}$$

In coating thin film at high velocity, the meniscus retreats into the gap zone, making it impossible to trace the shape with a Cartesian coordinate system. We, thus, use curvilinear coordinates to obtain

$$\begin{aligned} \sigma\frac{d}{dx}\left[\frac{h_{xx}}{(1+h_x^2)^{3/2}}\right] &= \sigma\frac{dH}{ds}\frac{1}{\cos\theta} \\ &= f_s(s) + f_{un}(s,t) \end{aligned} \tag{33}$$

$$f_s = \rho\left(\frac{1}{5}\frac{U^2}{h} - \frac{6}{5}\frac{F_0^2}{h^3}\right)\sin\theta - 3\mu\left(\frac{U}{h^2} - \frac{F_0}{h^3}\right)\cos\theta \tag{34}$$

$$\begin{aligned} f_{un} &= \frac{\rho}{h}\left(F_{0t} - \frac{\partial^2}{\partial t^2}\int_{s_1}^{s} h\cos\theta ds\right)\cos\theta \\ &+ \rho\left[h_{ta}\left(\frac{2}{5}\frac{U}{h} - \frac{12}{5}\frac{F_0}{h^2}\right)\cos\theta + \frac{\partial}{\partial t}\int_{s_1}^{s} h\cos\theta ds\frac{12}{5}\frac{F_0}{h^3}\sin\theta\right] \\ &- \mu\frac{3}{h^3}\frac{\partial}{\partial t}\int_{s_1}^{s} h\cos\theta ds\cos\theta \end{aligned} \tag{35}$$

where

$$\frac{d\theta}{\partial s} = H, \quad \frac{dh}{ds} = \sin\theta, \quad \frac{dx}{ds} = \cos\theta \tag{36}$$

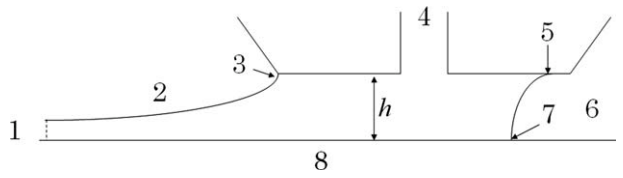

Figure 5. Flow domain with boundary conditions.

Figure 5 shows the flow domain boundaries. At the end of film flow (1), we assume the flow to be fully developed and impose the boundary condition

$$\frac{\partial h}{\partial t}+\frac{\partial}{\partial x}\int_0^h udy=0 \tag{37}$$

Downstream (2), we assume the air pressure to be zero. The static contact line attached to the downstream free surface (3) is pinned at the sharp edge of the die. In the inflow region, we assume the flow to be fully developed so that

$$Q_i=Q_{i0}+\varepsilon e^{j\,\varpi t} \tag{38}$$

where ϵ and ω are the amplitude and frequency, respectively, of the disturbance, and j is the imaginary unit. At the dynamic contact line (7), we use the empirical correlation to impose the condition[21]

$$\cos\alpha_{\text{dynamic}}=\cos\alpha_{\text{static}}-2Ca^{0.5}(\cos\alpha_{\text{static}}+1) \tag{39}$$

At the upstream gas-liquid interface (6), vacuum pressure P_v is usually applied in order to stabilize the coating bead, giving

$$P_v=P_{v0}+\varepsilon e^{j\,\varpi t} \tag{40}$$

At the static contact line attached upstream, the free surface (5) can move along the lip with static contact angle β. The pressure balance at the upstream free surface becomes[13]

$$h_u(x_4)p(x_4)+\sigma(\cos\alpha_{\text{dynamic}}+\cos(\beta-\theta_u))-h_u(x_4)p_v(t)=0 \tag{41}$$

At the substrate (8), we impose a web velocity condition

$$U=U_0+\varepsilon e^{j\,\varpi t} \tag{42}$$

We consider the effect of die vibrations to alter the gap height h such that

$$h=h_0+\varepsilon e^{j\,\varpi t} \tag{43}$$

Note that every equation given here was checked by technical computing software (Mathematica, Wolfram Research).

Frequency-response analysis

These nonlinear equation systems (Eqs. 21,25,29,33,36,37, and 41) are solved all together by a finite difference method with second-order approximation. The finite differences create residuals for these discretized equations at each node. When all variables are setup, the partial differential equations reduce to simultaneous algebraic equations for the nodal values of all field variables. The system of equations is nonlinear and sparse, and can be solved by Newton's method, which guarantees the correctness of the Jacobian matrix and the program in obtaining quadratic convergence. This discretized equation system at steady state is

$$R_\eta\Delta\eta=R \tag{44}$$

where R are residuals, η are variables, and the subscripts indicate partial derivatives. First, we evaluate all the variables at steady state, which is equivalent to all residuals being zero. Using a Taylor expansion, we predict the frequency response of the variables to disturbances around the steady state as

$$R_\eta\Delta\eta+R_{\dot\eta}\Delta\dot\eta+R_{\ddot\eta}\Delta\ddot\eta+R_\pi\Delta\pi+R_{\dot\pi}\Delta\dot\pi+R_{\ddot\pi}\Delta\ddot\pi=0 \tag{45}$$

where

$$\Delta\eta=\eta-\eta_{\text{steady}},\Delta\pi=\pi-\pi_{\text{steady}} \tag{46}$$

where π is a parameter of the coating process such as web velocity, vacuum pressure, flow rate, or coating gap, and the dot indicates a derivative with respect to time. To transform this into a state-space equation, we consider multiple variable arrangements

$$B_1\dot z=B_2z+Dk \tag{47}$$

where

$$z=(\Delta\eta,\Delta\dot\eta)^T,\quad k=(\Delta\pi,\Delta\dot\pi,\Delta\ddot\pi)^T \tag{48}$$

$$B_1=\begin{bmatrix}R_{\dot\eta} & R_{\ddot\eta}\\ I & 0\end{bmatrix}\quad B_2=\begin{bmatrix}-R_\eta & 0\\ 0 & I\end{bmatrix} \tag{49}$$

$$D=\begin{bmatrix}-R_\pi & -R_{\dot\pi} & -R_{\ddot\pi}\\ 0 & 0 & 0\end{bmatrix} \tag{50}$$

In Eq. 47, since the matrix B_1 is singular, we solve the matrix equation by the direct method, which is efficient and does not use complex variables.[6] First, suppose only one parameter suffers a disturbance, so that

$$\begin{aligned}&\Delta\eta=\varepsilon\delta e^{j\varpi t},\quad \Delta\dot\eta=j\varepsilon\varpi\delta\, e^{j\varpi t},\quad \Delta\ddot\eta=-\varepsilon\varpi^{\,2}\delta e^{j\varpi t}\\ &\Delta\pi=\varepsilon e^{j\varpi t},\quad \Delta\dot\pi=j\varepsilon\varpi\, e^{j\varpi t},\quad \Delta\ddot\pi=-\varepsilon\varpi^{\,2}e^{j\varpi t}\end{aligned} \tag{51}$$

where

$$\delta=\delta_r+j\delta_i \tag{52}$$

Using Eq. 51 and Eq. 52, the real and imaginary parts of Eq. 45 become two separate equations

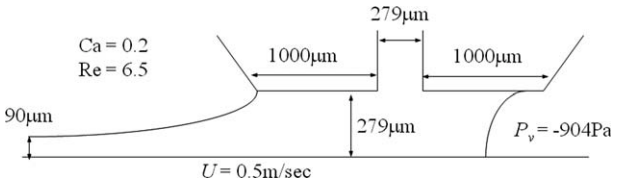

Figure 6. The geometry and parameters of the slot die.

$$\begin{aligned}\left(R_\eta - \varpi^2 R_{\ddot{\eta}}\right)\delta_r - \varpi R_{\dot{\eta}}\delta_i &= -\left(R_\pi - \varpi^2 R_{\ddot{\pi}}\right) \\ &= m_1\delta_r - m_2\delta_i = -n_1 \\ j\varpi R_{\dot{\eta}}\delta_r + j\left(R_\eta - \varpi^2 R_{\ddot{\eta}}\right)\delta_i &= -j\varpi R_{\dot{\pi}} \\ &= jm_2\delta_r + jm_1\delta_i = -jn_2 \end{aligned} \quad (54)$$

Using a matrix formulation, we can rearrange these equations to

$$\begin{bmatrix} m_1 & -m_2 \\ m_2 & m_1 \end{bmatrix}\begin{bmatrix} \delta_r \\ \delta_i \end{bmatrix} = \begin{bmatrix} -n_1 \\ -n_2 \end{bmatrix} \quad (55)$$

When we compare computational results with experimental data,[22] we find them to agree well.

Figure 6 shows geometric details of the slot die considered in this study. The coating gap is uniform, the static contact line at substrate and die is 62°, the characteristic length is assumed to be the same as the coating gap [2.79×10^{-4} m (h)], and the surface tension at the gas-liquid interface is fixed at 0.061 N/m. Thus, the Reynolds number Re is 6.5 and the capillary number Ca is 0.2 (assuming that the density of the liquid is 1190 kg/m^3). We computed the frequency response to disturbances of web velocity, inflow rate, vacuum pressure, and gap oscillations. In each case, the amplitudes of disturbance are 1% of the parameter value set, and do not create significant nonlinear effects.[23]

Figures 7–10 show frequency response analyses of changes induced in the film thickness at the asymptotic region of the coating film by disturbances. In each plot, the vertical axis is the gain in film thickness for each type of input disturbance and the horizontal axis is the frequency of the disturbance. Figures 7 and 8 the frequency response results show that oscillations in coating bead and meniscus have the characteristics of a low-pass filter; the gradient of the response curve suggests, since there is no peak, that the system operates as a first-order low-pass filter-—in other words, as a first-order lag process. In Figure 9, frequency response implies that the oscillations system have the characteristics of a band-pass filter; the slopes on the right and left sides differ, so the order of the two filters also differ. Figure 10 shows three peaks. Because their gradients are steeper than those in Figure 9, they might be regarded as resonant phenomena. However, the troughs between the peaks, which correspond to characteristics of the coating bead and meniscus, are relatively high and the peaks are not clearly separated, so each peak does not necessarily represent a separate resonant mode. In the next section, we use experimental modal analysis to decompose frequency properties according to bead and meniscus region, providing insights into the dynamic characteristics of the coating bead and meniscus.

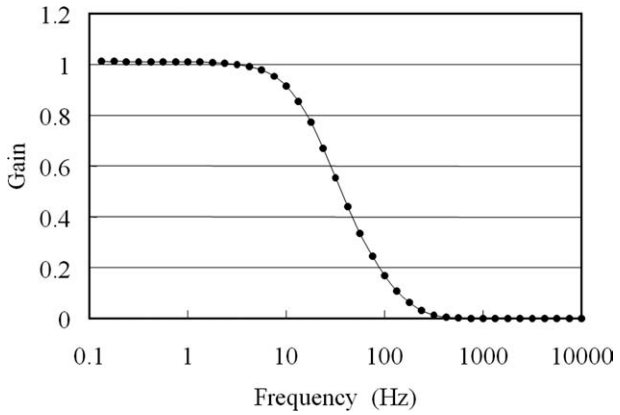

Figure 8. Frequency responses to inlet flow rate disturbance.

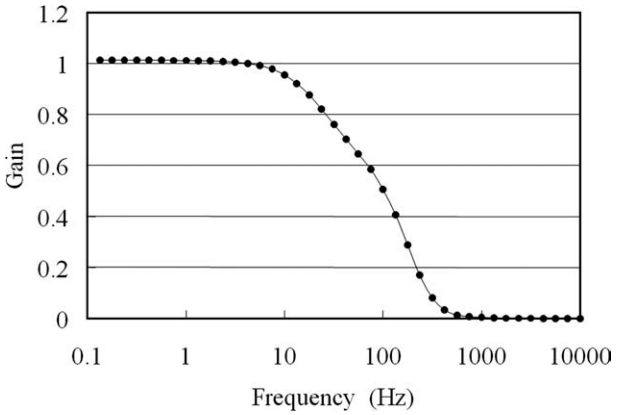

Figure 7. Frequency responses to web velocity disturbance.

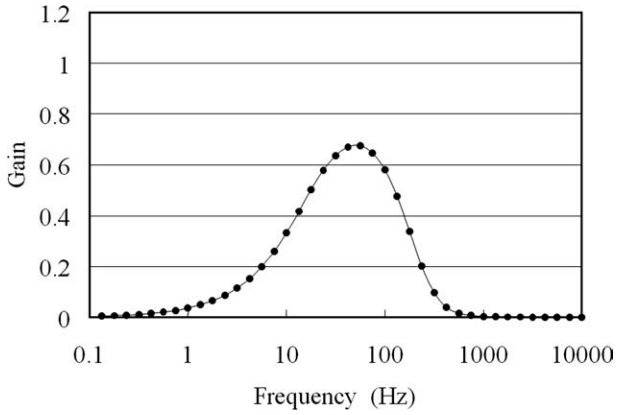

Figure 9. Frequency responses to vacuum pressure disturbance.

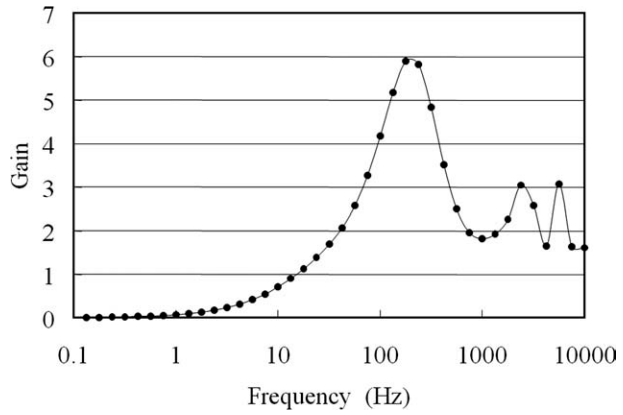

Figure 10. Frequency responses to coating gap oscillation.

Experimental modal analysis

Continuous flexible structures generally have multiple oscillation modes. Modal analysis provides certain eigenfunctions and eigenmodes that are equivalent to physical resonant modes. In dealing with symmetric, uniform, linear structures, we simply specify equivalent eigenmodes. However, in dealing with complex structures, it is complicated to specify modes, since many weak coupled modes exist. We, therefore, analyze a complicated coating bead and meniscus system by a substructure synthesis method[24] similar to experimental modal analysis.

Figure 11 shows a flow chart of disturbances. These disturbances vibrate the coating bead and induce variations in flow rate F_0 at the exit of the gap zone, which in turn induce variations in thickness h. The transfer function is

$$Transfer\ function = \frac{Output}{Input} \tag{56}$$

This equation indicates that frequency response results from multiplying the bead and meniscus transfer functions. To specify the transfer function, we derive a linearized unsteady equation by a perturbation method. As an example, we consider a concrete procedure using the meniscus region. By assuming that time-dependent terms in the film thickness, curvature, and other parameters are small enough to treat as perturbations, we obtain

$$h = h_s(x) + \varepsilon h_D(x,t) \tag{57}$$

$$h_s = h_\infty + \varepsilon h_1(x) \tag{58}$$

$$\sigma h_{xxx} = \sigma h_{s\,xxx}(x) + \sigma\varepsilon h_{Dxxx}(x,t) \tag{59}$$

$$U = U_s + \varepsilon U_D(t) \tag{60}$$

$$F_0 = F_S + \varepsilon F_D(t) \tag{61}$$

In Eqs. 57–61, ε has a small value, the S and D subscripts indicate steady and unsteady values, respectively, and the infinity subscript indicates the final coating thickness. Substituting these equations assuming that terms higher than second-order in ε are zero, we obtain the linearized equation

$$\sigma h_{Dxxx} = \rho\left(\frac{1}{5}\frac{U_S^2}{h_\infty} - \frac{6}{5}\frac{F_S^2}{h_\infty^3}\right)h_{Dx} - 3\mu\left(\frac{2U_S}{h_\infty^3} - \frac{F_S}{h_\infty^4}\right)h_D - 3\mu\left(\frac{U_D}{h_\infty^2} - \frac{F_D}{h_\infty^3}\right) + \rho\frac{1}{h_\infty}\left(F_{Dt} - \int_{x_1}^{x} h_{Dtt}dx\right) + \rho(h_{Dt}(x) - h_{Dt}(x_1))\left(\frac{2U_s}{5h_\infty} - \frac{12F_S}{5h_\infty^2}\right) - \mu\frac{3}{h_\infty^3}\int_{x_1}^{x} h_{Dt}dx \tag{62}$$

According to the methods of modal analysis, the response of each mode can be obtained using the superposition

$$h_D(x,t) = \sum_{n=1}^{n=\infty} Y_n(x)G_n(t,\tau_n(x)) \tag{63}$$

where Y is the orthogonal modal function of the meniscus mode shape, G is the time-dependent function, and τ is the phase lag.

Next, we consider the fixed condition of $x = L$ (meniscus endpoint) and $n = 1$ (one mode). To simplify the problem, we normalize Y_n at $x = L$ ($Y_n(L) = 1$). Substituting Eq. 63 into Eq. 62 gives the simplified equation

$$a_1\ddot{G}_1(t) + a_2\dot{G}_1(t) + a_3G_1(t) + a_4U_D + a_5\dot{F}_D + a_6F_D + a_7\dot{h}_D(x_1) = 0 \tag{64}$$

Since we do not have information about the modal shape of meniscus oscillation, we cannot estimate the coefficients a_i that contribute to Y. Instead, we specify these coefficients from the transfer function using curve-fitting. To adapt the equation system to the frequency domain, we define the variables and normalized parameters

$$\frac{G_1(t)}{h_S(L)} = g_1(\varpi)e^{j\varpi t} \tag{65}$$

$$\frac{U_D}{U_S} = g_U(\varpi)e^{j\varpi t} \tag{66}$$

$$\frac{F_D}{F_S} = g_F(\varpi)e^{j\varpi t} \tag{67}$$

$$\frac{h(x_1)_D}{h(x_1)_S} = g_h(\varpi)e^{j\varpi t} \tag{68}$$

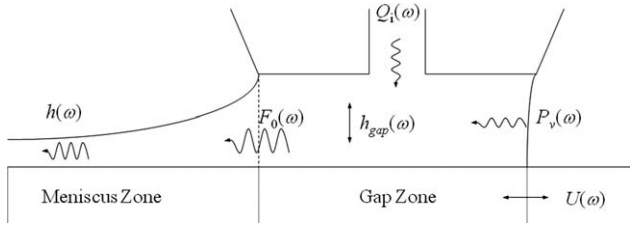

Figure 11. Flow chart of disturbances in coating bead and meniscus.

Substituting these equations into Eq. 64 gives

$$g_1(\varpi) = \frac{a_4}{-a_1\varpi^2 + a_2 j\varpi + a_3} g_U(\varpi) + \frac{a_5 j\varpi + a_6}{-a_1\varpi^2 + a_2 j\varpi + a_3} g_F(\varpi) + \frac{a_7 j\varpi}{-a_1\varpi^2 + a_2 j\varpi + a_3} g_h(\varpi) \tag{69}$$

The aforementioned equation shows the relationship between input (disturbance web velocity g_U, flow rate g_F, and gap oscillation g_h), and output (variation in thickness at the end of meniscus g_1) in the frequency domain. This equation system clearly has the same form as an n-order mode. In the bead region, the degree of freedom n is just 1 according to the governing equation, since the bead is surrounded by a fixed wall.

By the same procedure, we obtain the following coating bead region equation, which shows the relationship between disturbance and variation in flow rate at the exit of the coating gap

$$g_F(\varpi) = \frac{(b_4 j\varpi + b_5) j\varpi}{-b_1\varpi^2 + b_2 j\varpi + b_3} g_Q(\varpi) + g_Q(\varpi) \tag{70}$$

$$g_F(\varpi) = \frac{(-c_4\varpi^2 + c_5 j\varpi + c_6) j\varpi}{-c_1\varpi^2 + c_2 j\varpi + c_3} g_h(\varpi) + c_7 j\varpi g_h(\varpi) \tag{71}$$

$$g_F(\varpi) = \frac{(e_4) j\varpi}{-e_1\varpi^2 + e_2 j\varpi + e_3} g_U(\varpi) \tag{72}$$

$$g_F(\varpi) = \frac{(e_5) j\varpi}{-e_1\varpi^2 + e_2 j\varpi + e_3} g_{Pv}(\varpi) \tag{73}$$

where

$$\frac{Q_D}{Q_S} = g_Q(\varpi) e^{j\varpi t} \tag{74}$$

$$\frac{P_{vD}}{P_{vS}} = g_{Pv}(\varpi) e^{j\varpi t} \tag{75}$$

$$Q_i = Q_S + \varepsilon Q_D \tag{76}$$

$$P_v = P_{vS} + \varepsilon P_{vD} \tag{77}$$

These equations contain equivalent oscillator basis functions at each mode, suggesting that each transfer function consists of a through signal, a first- and second-order low/high-pass process and a combination system (band-pass), and, thus, implying that the systems are damped, resonant, or complex. We show these basic functional forms as

$$LowPass(1st) = \frac{c_1}{c_2 + j\varpi} \tag{78}$$

$$Highpass(1st) = \frac{c_1 j\varpi}{c_2 + j\varpi} \tag{79}$$

$$LowPass(2nd) = \frac{c_1}{-\varpi^2 + c_2 j\varpi + c_3} \tag{80}$$

$$HighPass(2nd) = \frac{c_1\varpi^2}{-\varpi^2 + c_2 j\varpi + c_3} \tag{81}$$

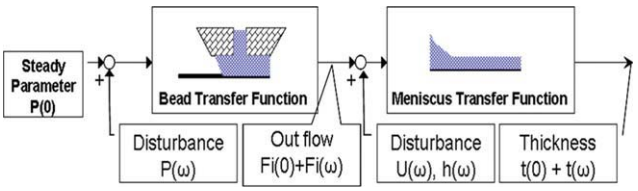

Figure 12. Flow chart of transfer functions in coating bead and meniscus.

[Color figure can be viewed in the online issue, which is available at wileyonlinelibrary.com.]

$$BandPass(1st) = \frac{c_1 j\varpi}{-\varpi^2 + c_2 j\varpi + c_3} \tag{82}$$

$$BandPass(2nd) = \frac{c_1 j\varpi^2}{\varpi^4 + c_2 j\varpi^3 + c_3\varpi^2 + c_4 j\varpi + c_5} \tag{83}$$

Generally, a first-order low-pass action is created from accumulating action, while second-order low/high-pass or band-pass systems are equivalent to the model having resonant phenomena since the denominators of the transfer function are equivalent to those of dynamic vibration systems (second-order mass-damping-spring model). However, band-pass filter might arise from a combination of a complex system involving a first-order low/high-pass filter. In this case, we consider the bead system as a single system, and, therefore, regard these equations as resonant phenomena.

Several methods exist for curve-fitting in the frequency domain, depending on system properties.[24] We use the simplified linear direct method, since we neglected nonlinear effects and lack information about resonant frequency. First, we define the error function between computational and modeling results as

$$\Lambda_{\mathrm{Re}} = \Gamma_{\mathrm{Re}}(\varpi) - \Omega_{\mathrm{Re}}(\varpi) \tag{84}$$

$$\Lambda_{\mathrm{Im}} = \Gamma_{\mathrm{Im}}(\varpi) - \Omega_{\mathrm{Im}}(\varpi) \tag{85}$$

where Γ is the modeling response function (equivalent to g_1 or g_F), Ω is the computational result found using the governing equation, and the subscripts *Re* and *Im* indicate real and imaginary parts of the value, respectively.

To determine the system function, we solve the set of linear algebraic equations, which contain the coefficients. We compute each modal equation separately, changing the frequency range to get the minimum error Λ.[25] To avoid an aliasing effect, we restrict the frequency to <1 kHz, a realistic value in industrial processes. Furthermore, we specify these coefficients while neglecting modes higher than the fourth.

Figure 12 shows how the transfer functions are related. Each disturbance parameter P (velocity, flow rate, vacuum pressure, gap oscillation) creates a variation in outflow according to the bead transfer function. Variations in outflow, web velocity, and gap oscillation create variations in film thickness according to the meniscus-transfer function.

Figures 13–16 show the results of curve-fitting to the bead and meniscus-transfer function. Circles show curve-fitting results; lines show computation results. Curve-fitting and computational results agree well, indicating that the modeling procedure appropriately predicts the dynamic system. Figure 13 shows that the coating bead compensates for

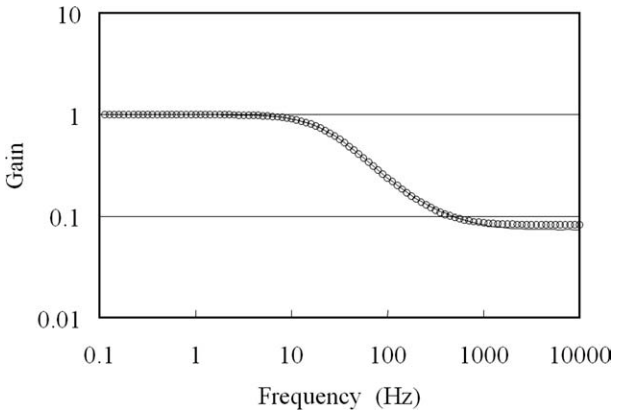

Figure 13. Curve fit result of bead transfer function to inflow rate disturbance.

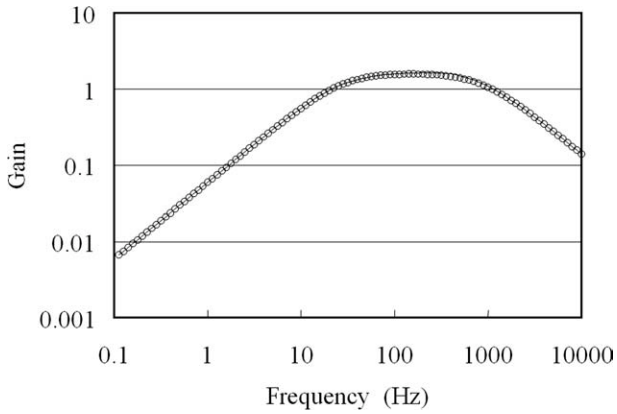

Figure 15. Curve fit result of bead transfer function to web velocity disturbance.

fluctuations in outflow rate resulting from disturbances such as from a flow integrator, particularly at frequencies >100 Hz.

Figure 14 shows that the most important disturbance to the coating bead is gap oscillation. Compared with the effect of other disturbances on the coating bead, the energy of the gap oscillation disturbance continues to rise in the high-frequency region. The disturbance must excite hidden minor modes in the high-frequency region, which usually suffers strong viscous damping. Figures 15 and 16 show similar variations in their respective transfer functions, which we categorize as resonant phenomena since the transfer functions (Eqs. 72 and 73) are equivalent to the band-pass filter function (Eq. 82), which has a resonant mode. The reason for their similarity is probably that both disturbances create a pressure field fluctuation in the coating bead: the web velocity creates a fluctuation by controlling Couette flow, while the vacuum pressure creates a fluctuation by controlling Poiseuille flow.

Next, we consider the meniscus-transfer functions. Figures 17–19 show that, at <1 kHz, considered to be the target frequency band, curve-fitting and computational results agree well. In Figures 17 and 18, the transfer function is of the low-pass type, but at higher frequencies the gradient changes slightly, implying the presence of multiple modes. Figure 18 shows that several resonant phenomena exist.

From these results, we can understand how the frequency response is created. First, the frequency response to a web velocity disturbance (Figure 7) consists of the product of the bead component (Figure 15), meniscus-outflow rate component (Figure 17), and meniscus-web velocity component (Figure 18). Hence, the roundness of the response curve in Figure 7 in the range 10–100 Hz is created by a bead component effect. Second, the frequency response to the flow rate disturbance (Figure 8) consists of the product of the bead inflow rate component (Figure 13) and meniscus-outflow rate component (Figure 17). Hence, the region of decay (10–100 Hz in Figure 8) is created by a bead component effect. The frequency response to a vacuum pressure disturbance (Figure 9) consists of the product of the bead vacuum component (Figure 16) and meniscus-outflow rate component (Figure 17). The reason for the asymmetric gradient of the response curve in Figure 9 is that the left-side curvature is created in the bead region, and the right-side curvature is created in the meniscus region. Third, the frequency response to gap oscillation (Figure 10) consists of the product of the bead gap component (Figure 14), meniscus-outflow rate component (Figure 17), and meniscus gap component (Figure 19). The main response is created in the bead

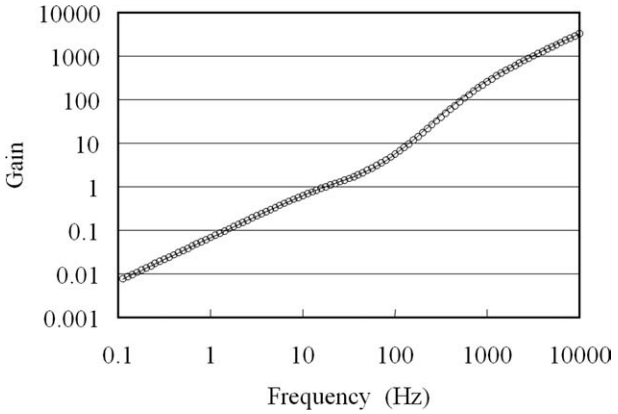

Figure 14. Curve fit result of bead transfer function to gap oscillation disturbance.

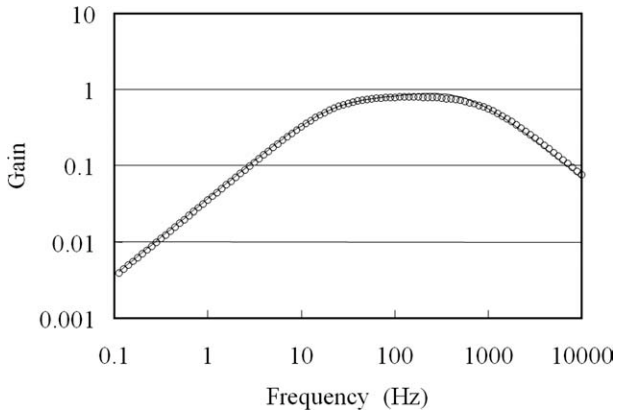

Figure 16. Curve fit result of bead transfer function to vacuum pressure disturbance.

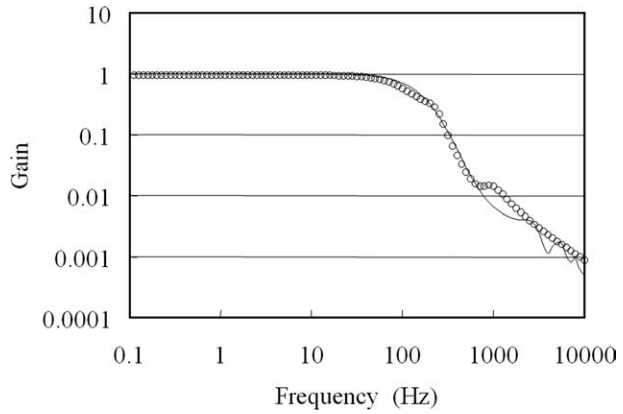

Figure 17. Curve fit result of meniscus-transfer function to outflow rate disturbance.

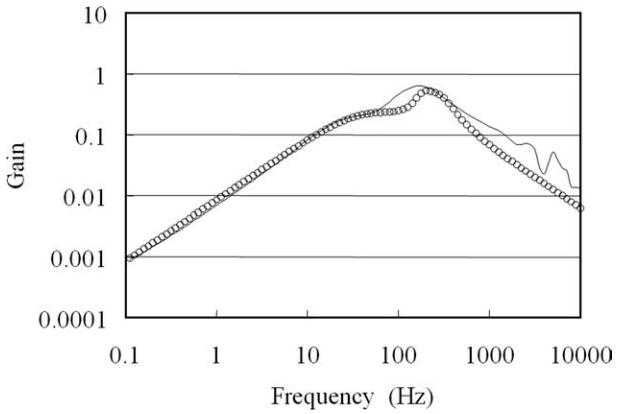

Figure 19. Curve fit result of meniscus-transfer function to gap oscillation.

region, which enables higher modes to be fully excited since the disturbance level is intense in the high-frequency region.

In the meniscus region, the dominant transfer function is the one describing the outflow rate disturbance. Since coating defects from gap oscillations are the most serious problem in reality, the product of the gap oscillation and outflow rate functions constitute a good example. We next consider the decomposition of each mode of the transfer function to understand the characteristics of the meniscus oscillation system.

Figure 20 shows the results obtained by decomposing each mode using the relationship of Eq. 63. At <1 kHz, there are three modes: one low-pass type and two low-pass types that also have a resonant point. From these results, we find that a single-response peak in the frequency response (for example, Figure 10) consists of multiple eigenmodes (peaks and low-pass filter processes).

Next, we consider the resonant phenomena. Figures 21–23 show the results of meniscus mode shape computations at the dominant frequency point. The meniscus shape is excited by gap oscillations and decomposes into real and imaginary amplitudes equivalent to the minimum and maximum amplitudes in the time domain. In Figure 21, the surface of the meniscus (2.28–3.00×10^{-3} m) moves coherently; in other words, the meniscus is periodically squeezed. Since this squeeze mode does not exhibit a peaked response, we presume that viscous damping is the dominant effect.[26] The other two modes are sinuous, and move in wave-like string vibrations.[27] Comparison of Figures 22 and 23 shows that, although the variation in thickness of the third mode at $\sim 4.00 \times 10^{-3}$ m is smaller than that of the second mode, the variation in film thickness in the meniscus zone is significant enough to create other coating defects. Thus, it is important to analyze the dynamic coating meniscus behavior near the die lip region, as well as at the film endpoint.

Figure 24 compares the characteristics of sinuous modes and capillary waves. Computational results agree with the capillary wave first-order approximation.[28] In other words, the sinuous modes are themselves capillary waves. Note that the modal structures are available for the case of no coating defects such as ribbing, barring, and swelling, since the meniscus shape contains 2-D/3-D deformation in these cases.

Conclusion

Slot coating is one of the preferred methods for creating high-precision coated products. For product uniformity, it is important to consider the effects of disturbances and to

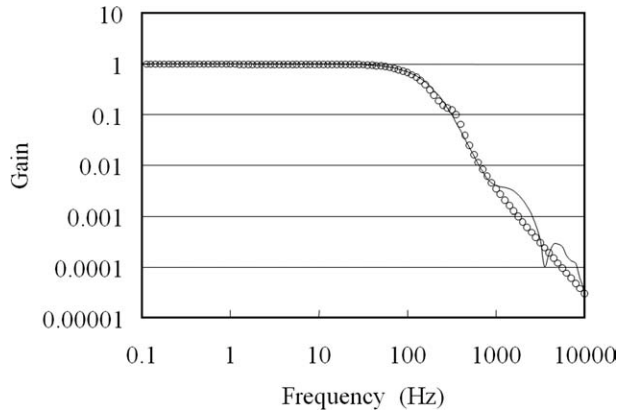

Figure 18. Curve fit result of meniscus-transfer function to web velocity disturbance.

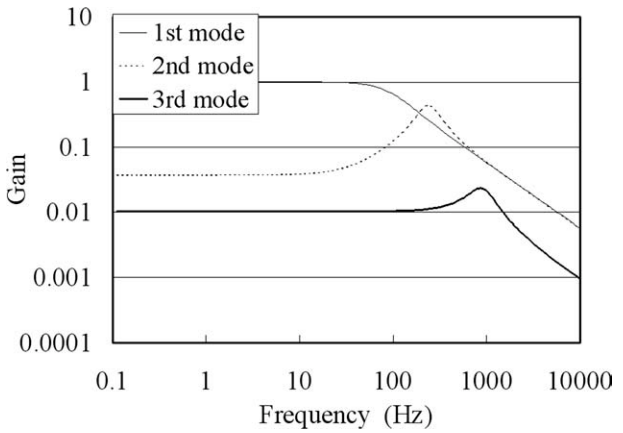

Figure 20. Curve fit result of decomposed meniscus-transfer function to outflow rate disturbance.

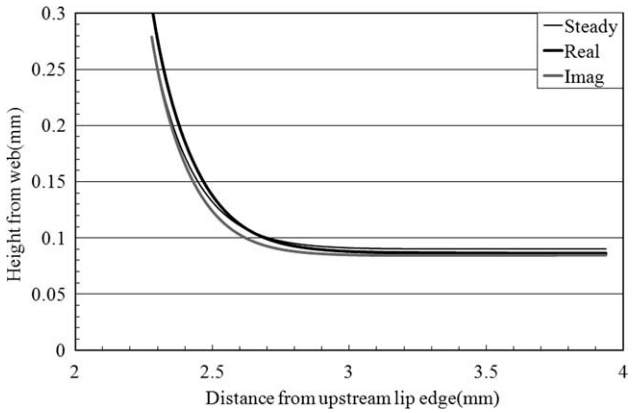

Figure 21. Frequency response of first-mode meniscus shape to gap oscillation (10Hz, ε = 10%).

resolve those disturbances immediately. Frequency response analysis has been used to predict variations in thickness caused by several types of disturbance. However, such analysis shows merely the resulting response, and not the root causes. Another difficulty is that previous frequency response analyses considered only the final thickness point, and not the meniscus or gap zone. Furthermore, they regarded the single-peak response in the frequency domain as one physical resonant mode.

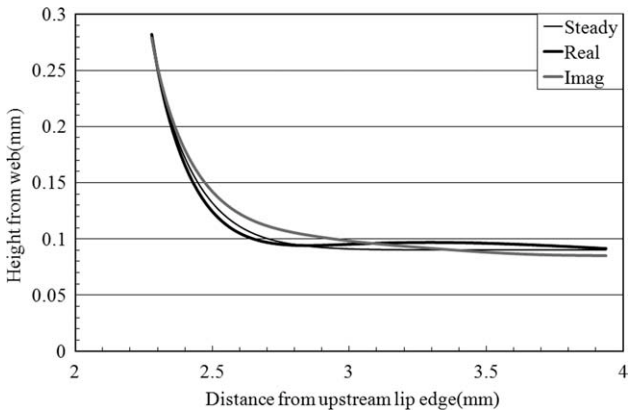

Figure 22. Frequency response of second-mode meniscus shape to gap oscillation (200Hz, ε = 1%).

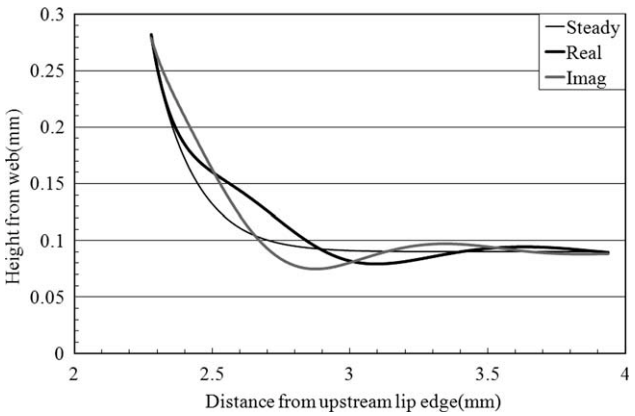

Figure 23. Frequency response of third-mode meniscus shape to gap oscillation (750Hz, ε = 1%).

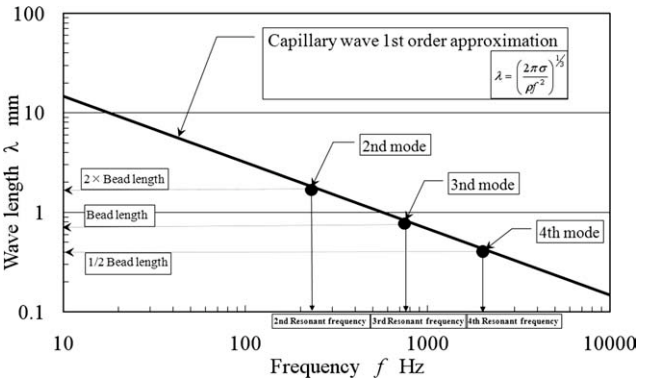

Figure 24. Comparison with capillary wave first-order approximation.

In this work, we proposed an efficient 1-D unsteady equation to reduce time cost. To examine the frequency response of a slot coating, we introduced an empirical modal analysis approach. The model has an oscillator basis with a transfer function assumed from a linearized governing equation. The coefficients of the basis model are found by curve-fitting. Each mode can be decomposed into two types of mode shape: a squeeze mode related to viscous behavior and sinuous modes that are identical to capillary waves. By observing the meniscus shapes in each mode, we find that, in the third mode near the lip edge, significant fluctuations exist that induce coating defects.

Literature Cited

1. Schweizer PM, Kistler SF. *Liquid Film Coating*. New York: Chapman & Hall; 1997.
2. Wowk V. *Machinery. Vibration Measurement and Analysis*. New York: McGraw-Hill, Inc; 1991.
3. Durst F, Raszillier H. *Advances in Coating and Drying of Thin Films. 3rd European Coating Symposium 1999*. Germany: Shaker Verlag GmbH; 1999.
4. Kalman RE. a new approach to linear filtering and prediction problem. *J Basic Eng*. 1960;82:35–45.
5. Van Abbenyen W, Goetmaeckers B, Van de Vijver H, Bußmann H, Beck D. Experimental verification of the calculated frequency response of a multilayer slide coating operation. Proceedings of the AIChE Spring Meeting; 1990.
6. Christodoulou KN. *Computational Physics of Slide Coating Flow*. Minneapolis, MN: University of Minnesota; 1990. PhD Thesis.
7. Cai J. *Coating Rheology: Measurements, Modeling, and Applications*. MN: University. of Minnesota; 1994. PhD Thesis.
8. Gates ID. *Slot Coating Flows: Feasibility, Quality*. MN: University of Minnesota; 1999. PhD Thesis.
9. Musson LC. *Two-Layer Slot Coating*. MN: University of Minnesota; 2001. PhD Thesis.
10. Katagiri Y, Scriven LE. Supercomputer aided analysis of transient response. Proceedings of the AIChe Annual Meeting; 1986.
11. Landau L, Levich B. Dragging of a liquid by a moving plate. *Acta Physicochim(USSR)*. 1942;17:42–54.
12. Gardner GC, Adebiyi GA. The liquid film left behind by a large bubble in a sloping channel. *Chem Eng Sci*. 1974;29:461–473.
13. Higgins BG. *Capillary Hydrodynamics and Coating Beads*. MN: University of Minnesota; 1980. PhD Thesis.

14. Kheshgi HK. The Motion of Viscous Liquid Films. MN: University of Minnesota; 1983. PhD Thesis.
15. Schlichting H. *Boundary Layer Theory*. 8th ed. New York: Springer; 2000.
16. Sartor L. *Slot Coating: Fluid Mechanics and Die Design*. MN: University of Minnesota; 1990. PhD Thesis.
17. Kapitza P. Wave flow of thin layers of a viscous fluid: I. free flow. *Zh Eksp Teor Fiz*. 1948;18:3–28.
18. Shkadov V. Wave flow regimes of a thin layer of viscous fluid subject to gravity. *Izv Ak Nauk SSSR Mekh Zhidk Gaza, Mekh Zhi Gaza*. 1967;1:43–51.
19. Chang HC. Wave evolution on a falling film. *Ann Rev Fluid Mech*. 1994;26:103–136.
20. Panton RL. *Incompressible Flow*. New York: John Wiley & Sons; 1996.
21. Bracke M, De Voeght F, Joos P. The Kinetics of wetting: the dynamic contact angle. *Prog Colloid Polym Sci*. 1989;79:142–149.
22. Joos FM. A simple model of frequency response for slot coaters. Proceedings of the 3rd European Coating Symposium; 1999.
23. Tsuda T. Dynamic response analysis and control of slot coating. *J Fluid Sci Technol*. 2009;4:735–745.
24. Nagamatsu A. *Modal Analysis*. Tokyo: Baifukan; 1985.
25. Wang S, Sate H, O-hori M. New approaches to the modal analysis for machine tool structure. *Trans ASME*. 1984;106:40–47.
26. Maia NMM, Silva JMM. *Theoretical and Experimental Modal Analysis*. Philadelphia: Taylor & Francis; 1998.
27. Lord Rayleigh. *Theory of Sound*. New York: Dover, 1945.
28. Lamb H. *Hydrodynamics*. New York: Cambridge Univ. Press; 1932.

Manuscript received June 21, 2009, and revision received Nov. 3, 2009.